



# Dynamic susceptibility-contrast magnetic resonance imaging with contrast agent leakage correction aids in predicting grade in pediatric brain tumours: a multicenter study

Stephanie B. Withey<sup>1,2,3</sup> · Lesley MacPherson<sup>4</sup> · Adam Oates<sup>4</sup> · Stephen Powell<sup>3</sup> · Jan Novak<sup>2,3,5</sup> · Laurence Abernethy<sup>6</sup> · Barry Pizer<sup>7</sup> · Richard Grundy<sup>8</sup> · Paul S. Morgan<sup>8,9,10</sup> · Simon Bailey<sup>11</sup> · Dipayan Mitra<sup>12</sup> · Theodoros N. Arvanitis<sup>2,3,13</sup> · Dorothee P. Auer<sup>10,14,15</sup> · Shivaram Avula<sup>6</sup> · Andrew C. Peet<sup>2,3,16</sup>

Received: 29 October 2020 / Revised: 31 August 2021 / Accepted: 11 December 2021 / Published online: 15 March 2022  
© The Author(s) 2022

## Abstract

**Background** Relative cerebral blood volume (rCBV) measured using dynamic susceptibility-contrast MRI can differentiate between low- and high-grade pediatric brain tumors. Multicenter studies are required for translation into clinical practice.

**Objective** We compared leakage-corrected dynamic susceptibility-contrast MRI perfusion parameters acquired at multiple centers in low- and high-grade pediatric brain tumors.

**Materials and methods** Eighty-five pediatric patients underwent pre-treatment dynamic susceptibility-contrast MRI scans at four centers. MRI protocols were variable. We analyzed data using the Boxerman leakage-correction method producing pixel-by-pixel estimates of leakage-uncorrected ( $rCBV_{uncorr}$ ) and corrected ( $rCBV_{corr}$ ) relative cerebral blood volume, and the leakage parameter,  $K_2$ . Histological diagnoses were obtained. Tumors were classified by high-grade tumor. We compared whole-tumor median perfusion parameters between low- and high-grade tumors and across tumor types.

**Results** Forty tumors were classified as low grade, 45 as high grade. Mean whole-tumor median  $rCBV_{uncorr}$  was higher in high-grade tumors than low-grade tumors (mean  $\pm$  standard deviation [SD] =  $2.37 \pm 2.61$  vs.  $-0.14 \pm 5.55$ ;  $P < 0.01$ ). Average median rCBV increased following leakage correction ( $2.54 \pm 1.63$  vs.  $1.68 \pm 1.36$ ;  $P = 0.010$ ), remaining higher in high-grade tumors than low grade-tumors. Low-grade tumors, particularly pilocytic astrocytomas, showed T1-dominant leakage effects; high-grade tumors showed T2\*-dominance (mean  $K_2 = 0.017 \pm 0.049$  vs.  $0.002 \pm 0.017$ ). Parameters varied with tumor type but not center. Median  $rCBV_{uncorr}$  was higher (mean = 1.49 vs. 0.49;  $P = 0.015$ ) and  $K_2$  lower (mean = 0.005 vs. 0.016;  $P = 0.013$ ) in children who received a pre-bolus of contrast agent compared to those who did not. Leakage correction removed the difference.

**Conclusion** Dynamic susceptibility-contrast MRI acquired at multiple centers helped distinguish between children's brain tumors. Relative cerebral blood volume was significantly higher in high-grade compared to low-grade tumors and differed among common tumor types. Vessel leakage correction is required to provide accurate rCBV, particularly in low-grade enhancing tumors.

**Keywords** Blood volume · Brain · Children · Dynamic susceptibility-contrast magnetic resonance imaging · Leakage correction · Magnetic resonance imaging · Multicenter · Perfusion · Tumor

## Introduction

Dynamic susceptibility-contrast MRI is a technique to measure perfusion in the brain. It involves the injection of a contrast agent during rapid MRI scanning, resulting in T2- or T2\*-weighted signal changes as the bolus of contrast agent passes through the intravascular space. Relative cerebral blood volume (rCBV) can be calculated by integrating the contrast agent concentration–time curve and is usually

✉ Andrew C. Peet  
a.peet@bham.ac.uk

Extended author information available on the last page of the article

reported in tumors as normalized to normal white matter [1, 2]. Relative cerebral blood volume has been shown to be useful for grading pediatric brain tumors [1, 2], monitoring treatment response [3], differentiating recurrent/residual tumor from treatment effect and providing markers of long-term prognosis [4]. Studies are usually performed at a single center, so there is a need to boost study numbers via multicenter studies and demonstrate that the technique is reproducible across sites and scanners to inform its use in clinical practice.

Conversely to adult brain tumors, many low-grade pediatric brain tumors display significant contrast enhancement on T1-weighted images [5]. Calculation of rCBV assumes that the blood–brain barrier remains intact. This is often not the case in brain tumors. Contrast agent leakage from the intravascular to the extravascular extracellular space results in an increase in MR signal from T1 shortening and underestimation of rCBV. Conversely, T2 and T2\* effects arise when there are changes in susceptibility differences between tissue compartments, reducing the MR signal so that it does not recover to baseline. This results in overestimation of rCBV. T1 effects can be reduced by administering a contrast agent pre-bolus [6, 7], by careful choice of pulse sequence parameters [6] or by post-processing methods [8–10]. A lack of agreement on the optimum acquisition technique leads to variations in protocols across centers and challenges for multicenter studies.

Following identification of a brain tumor on MRI, most children undergo biopsy or surgical resection. Some brain tumor types, such as diffuse intrinsic pontine gliomas [11], cannot be biopsied or undergo surgery because of their midline position. In addition, histopathological diagnosis has its limitations — results can be inconclusive or require central review, leading to increased waiting times for a diagnosis [12]. Treatment decisions are made based on tumor type, grade, molecular subtype, spread and age and fitness of the patients.

Advanced MRI techniques, such as magnetic resonance (MR) spectroscopy [12] and diffusion-weighted imaging [13], have been shown to increase accuracy in diagnosis compared to conventional MRI, resulting in increased confidence of radiological reporting. Early noninvasive diagnosis using advanced MRI can provide additional information and confidence in diagnoses compared to standard MRI alone, and is particularly useful in cases where biopsy/surgery is not an option or histological results are delayed. It can also inform the optimal biopsy site and allow for timely family discussions and organization of treatment.

Single-center dynamic susceptibility-contrast MRI studies [1, 2, 14, 15] have shown significantly higher rCBV associated with high-grade pediatric brain tumors, but patient numbers are small. In addition, differences in MR scanners

and protocols mean that parameters are not always comparable among centers. There is a need for multicenter pediatric studies to investigate the effect that differences in scanners and protocols have on perfusion parameters in order to develop robust biomarkers that can be used clinically to help with noninvasive tumor grading. The aims of this study were to (1) compare dynamic susceptibility-contrast MRI parameters in newly diagnosed pediatric low- versus high-grade tumors, with and without leakage correction; and (2) compare data acquired at multiple centers using varying dynamic susceptibility-contrast MRI protocols. We hypothesized that rCBV acquired from multicenter dynamic susceptibility-contrast MRI studies of children's brain tumors differs between high- and low-grade tumors and that leakage correction is important in determining rCBV.

## Materials and methods

This study was approved by the East Midlands–Derby research ethics committee (NRES REC ref.: 04/MRE04/41) and was performed in accordance with the ethical standards as laid down in the 1964 Declaration of Helsinki (and as revised in 1983). Informed parental consent was obtained from all subjects. Suitable patients were those undergoing dynamic susceptibility-contrast MRI scans with a primary brain tumor where histological data — tumor type and grade — were subsequently obtained. We anonymized the dynamic susceptibility-contrast and clinical MRI scans and uploaded them to the Children's Cancer and Leukaemia Group [16] Functional Imaging Database.

## Magnetic resonance imaging protocols

We acquired data from four centers that used six different MRI scanners. The protocols on each scanner are summarized in Table 1. Although dynamic susceptibility-contrast and clinical protocols were recommended by the European Society for Paediatric Oncology [17], centers chose and set up their own scanner-dependent protocols. Most centers used a gradient echo echoplanar imaging sequence with variable time to repetition (TR). Flip angles varied, with a low flip angle chosen to minimize T1-leakage effects on the MR signal. Scanning continued for a minimum of 70 s. While most centers covered the whole brain, this was not universal. Spatial resolution was variable. One center predominantly used the sensitivity-encoded Philips sPRESTO (principles of echo-shifting with a train of observations) sequence [18].

Gadolinium-containing contrast agent was administered via power injector through a cannula inserted into a suitable vein. Contrast agent brand, dose and injection rate are summarized (Table 1). Centers 1 and 3 consistently gave a pre-bolus of 50% of total dose and 1 mL, respectively,

**Table 1** Summary of seven dynamic susceptibility-contrast MRI protocols run across six scanners at four centers in this multicenter study

Center	1		2	3	4		
Scanner type	Siemens Avanto	Philips Achieva	Siemens Verio	Philips Achieva	Philips Achieva	Philips Achieva	Philips Achieva
Field strength	1.5 T	3 T	3 T	3 T	1.5 T	3 T	3 T
Head coil	12-element head	32-channel	32-channel	SENSE head-8	SENSE-NV-16	SENSE head-8	SENSE head-8
Sequence	GE-EPI	GE-EPI	GE-EPI	GE-EPI	sPRESTO	sPRESTO	GE-EPI
TR (ms)	1,490–1,643	1,830–1,865	1,570	1,666–2,343	16.7–17.2	15.5–16.0	582–1,866
TE (ms)	40	40	29	40	24.7–25.2	23.5–24.0	18.4–40.0
Flip angle (°)	20	20	45	75	7	7	20–40
Slice thickness (mm)	5.0	3.5	3.5	4.0	3.5	3.5	3.5–7.0
No. slices	19–21	30	16	25–35	30–36	30–34	30
No. dynamics	60	60	60	40	60	60	40–60
Field-of-view (mm)	230×230	240×240	220×220	224×224	220×220	230×230	240×240
Matrix	96×96	96×96	64×64	128×128	64–80×64–80	128×128	96×96
SENSE?	Y	Y	N	Y	Y	Y	Y
Temporal resolution (s)	1.5–1.6	1.8–1.9	1.6	1.7–2.3	1.3–1.6	1.2–1.4	0.6–1.9
Total scan time (s)	90–99	110–112	94	67–94	77–94	71–83	70–118
Pre-bolus	Y	Y	N	Y	Y (n=12), N (n=15), NA (n=9)		
Pre-bolus dose	Half	Half	–	1 mL	Range = 0.3–2.0 mL (10% of dose)		
Injection rate (mL/s)	3	3	6	3	3	3	3
Contrast agent	Dotarem	Dotarem	Dotarem	Dotarem	Magnevist (n=20), Gadovist (n=10), NA (n=6)		
No. patients	8	3	12	26	15	16	5

*GE-EPI* gradient echo echoplanar imaging, *n* number, *N* no, *NA* not available, *No.* number, *SENSE* sensitivity encoding, *sPRESTO* sensitivity-encoded Philips principles of echo-shifting with a train of observations, *T* tesla, *TE* time to echo, *TR* time to repetition, *Y* yes

administering the total dose of contrast in two stages — a pre-bolus for minimization of T1 effects followed by a second dose during the dynamic susceptibility-contrast data acquisition. An injection rate of 3 mL/s was recommended to minimize dispersion of the contrast agent bolus [17] and was used by all sites except one, which used a higher injection rate of 6 mL/s. Each injection was followed by up to 10 mL of saline. Center 2 did not employ a pre-bolus; at center 4, a pre-bolus of 10% of the total dose was administered to some children, depending on scanner, child's age and whether the child was scanned under general anesthetic. Injection details were not recorded for nine patients.

## Histology

Children underwent surgical resection or biopsy following MRI. Histological diagnoses were obtained locally. Tumors were classified and graded according to World Health Organization guidance available at the time [19–21] and were subsequently classified as low-grade (I and II) or high-grade (III and IV).

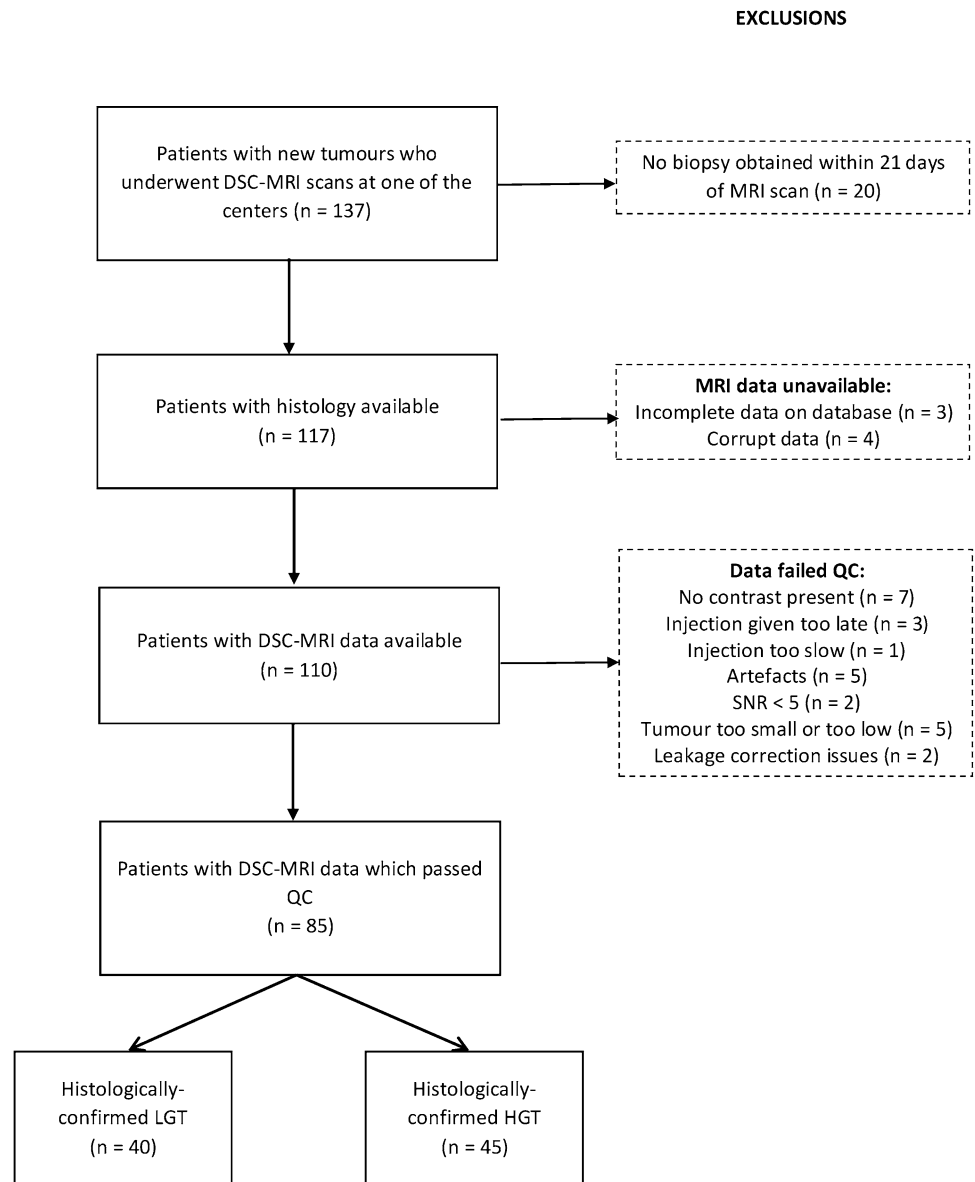
## Data analysis

We checked the MRI data downloaded from the central database for quality and completeness. We rejected data if scans were missing from the database, the contrast agent injection was administered late or slow so that there was insufficient acquisition to view the bolus passage, there were problems loading the data into the analysis software, or there were significant image artifacts or difficulties applying leakage-correction (Fig. 1).

Dynamic susceptibility-contrast analysis was performed using in-house software written in the Python programming language (v. 2.7). Pixel averaging using a 3×3 Gaussian kernel was performed prior to extracting signal–time curves from the dynamic susceptibility-contrast time-course on a pixel-by-pixel basis. Signal–time curves were converted to change in T2\* relaxation time,  $\Delta R_2^*$ :

$$\Delta R_2^* (t) = -\frac{1}{TE} \ln \left( \frac{S(t)}{S(0)} \right) \quad (1)$$

**Fig. 1** Flow diagram shows participants included in the study and reasons for exclusions. *DSC-MRI* dynamic susceptibility-contrast magnetic resonance imaging, *HGT* horizontal gene transfer, *LGT* lateral gene transfer, *QC* quality criteria, *SNR* signal-to-noise ratio



$S(t)$  and  $S(0)$  are the signal intensities at time  $t$  and baseline, respectively;  $TE$  is the time-to-echo of the dynamic susceptibility-contrast sequence.  $S(0)$  was calculated by averaging the signal from the first 6 time points. Pixel-by-pixel uncorrected cerebral blood volume ( $CBV_{uncorr}$ ) values were calculated by integrating over the  $DR2^*$ -time curves. Leakage-corrected  $DR2_{corr}^*$ -time curves were calculated using the Boxerman method, which also estimates the leakage-correction parameter,  $K_2$  [8–10]. This model aims to correct for both T1 and T2\* effects arising from contrast agent extravasation.

$$\Delta R_{2,corr}^*(t) = \tilde{\Delta R}_2^*(t) + K_2 \int_0^t \overline{\Delta R}_2^*(t') dt' \quad (2)$$

$\tilde{\Delta R}_2^*(t)$  is the uncorrected  $DR2^*$ ,  $\overline{\Delta R}_2^*(t')$  is the  $DR2^*$  obtained over the whole non-contrast-enhanced brain, therefore providing an estimate of  $DR2^*$  without allowing for leakage.  $K_2$  is a term reflecting the effects of leakage on both T1 and T2\* and is estimated by least-squares fitting the uncorrected  $DR2^*$  to:

$$\tilde{\Delta R}_2^*(t) \equiv K_1 \cdot \overline{\Delta R}_2^*(t) - K_2 \int_0^t \overline{\Delta R}_2^*(t') dt' \quad (3)$$

Positive  $K_2$  indicates that T1 effects dominate the resulting signal–time curve, while negative  $K_2$  indicates T2\*-dominant effect [9].  $K_1$  is a constant of proportionality.

Pixels were included in  $\overline{\Delta R}_2^*(t)$  as non-contrast-enhanced brain if they were not located in a ventricle, if the average signal of the last 10 time points was less than the average

plus the standard deviation in the baseline and if the average baseline signal intensity was greater than background noise. A manually input threshold for each patient differentiated ventricle from surrounding brain tissue.

Corrected cerebral blood volume ( $CBV_{\text{corr}}$ ) was calculated by integrating over leakage-corrected  $DR2^*$ -time curves,  $DR2_{\text{corr}}^*(t)$ . Maps of uncorrected and corrected cerebral blood volume and  $K_2$  were produced for each patient.

## Regions of interest

At center 1, a high-resolution T2-weighted turbo spin-echo scan with the same coverage as the dynamic susceptibility-contrast scan was acquired for defining regions of interest (TR/TE=4,000/100 ms, matrix = 144×144). At other centers T2-weighted and post-gadolinium T1-weighted clinical scans were downloaded from the central database for each patient depending on availability. Scans that did not have the same coverage as the dynamic susceptibility-contrast scan were reformatted and registered to the dynamic susceptibility-contrast images using an automatic affine transformation in the MERIT module in MeVisLab (v. 2.8.2; MeVis Medical Solutions AG, Bremen, Germany). After viewing the whole image set available for each case to clarify the tumor margins, whole-tumor regions of interest, excluding areas of cyst and vessels, were defined using MRICro [22] by a Clinical Scientist with 15 years of experience (S.B.W.) trained by a Consultant Pediatric Radiologist with 17 years of experience (L.M.). If there was any doubt as to whether abnormal tissue was tumor, it was not included in the region of interest. Fourteen randomly selected patients had regions of interest redrawn by a Consultant Radiologist with 7 years of experience (A.O.) to assess reproducibility.

Regions of interest were also defined in supratentorial normal-appearing cerebral white matter. Mean white matter cerebral blood volume was calculated for each child and used to normalize  $CBV_{\text{uncorr}}$  and  $CBV_{\text{corr}}$  maps. We then applied tumor regions of interest as a mask to the white-matter-normalized rCBV maps. Whole-tumor volumes were calculated by multiplying the number of voxels in the whole-tumor region-of-interest by the voxel volume. We calculated median, standard deviation, minimum, maximum, skewness and kurtosis of normalized whole-tumor uncorrected and corrected rCBV and  $K_2$ . We further divided the tumors listed in Table 2 into five groups by type: pilocytic astrocytomas, medulloblastomas, ependymomas, along with the less common high- and low-grade tumors grouped together as “other high-grade tumors” and “other low-grade tumors,” respectively. We calculated percentiles and produced histograms showing the distribution of whole-tumor parameters. Average rCBV<sub>uncorr</sub>, rCBV<sub>corr</sub> and  $K_2$  histograms were calculated for each of the five tumor groups.

## Statistical analysis

Statistical analyses were performed using SPSS (v. 2.5; IBM, Armonk, NY). A Shapiro-Wilk test was performed to test for normality. Spearman correlation was used to test for relationships between variables. We used a Wilcoxon signed-rank test to examine differences between parameters obtained from regions of interest defined by different operators. Kruskal-Wallis was performed to test for differences in parameters between the low- and high-grade tumor groups, among data acquired at different centers and among the five tumor groups. We also investigated sensitivity and specificity for distinguishing tumors as high- or low-grade using the median of each parameter as a cut-off.

## Results

The flow of participants through the study and reasons for exclusion are shown in Fig. 1. Table 1 summarizes the protocols of the four centers at which the 85 eligible children were scanned. Children were scanned between November 2005 and May 2017. Table 2 summarizes the demographics and diagnoses of eligible children. Data are shown for the most common tumor types, with the least common low- and high-grade tumors grouped together, respectively. Forty-five and 40 tumors were classified as high- and low-grade, respectively. Eleven, 12, 26 and 36 children were scanned at centers 1, 2, 3 and 4, respectively. The median time between the date of MRI scan and tissue being taken was 2 days (range 0–20 days). Forty-one children underwent complete macroscopic resection, 27 underwent incomplete resection and 17 underwent biopsy.

Wilcoxon signed-rank tests on whole-tumor median metrics — rCBV<sub>uncorr</sub>, rCBV<sub>corr</sub> and  $K_2$  — obtained from regions of interest defined by two separate operators to assess reproducibility ( $n=14$ ) showed no significant differences between the defined regions of interest ( $P>0.05$  in all cases). There were no significant differences between the proportions of low- and high-grade tumors scanned at each center compared to those across the whole cohort ( $P=0.16$ ). There was no significant difference between whole-tumor median parameters obtained at 1.5-tesla (T) and 3 T or between those obtained from scans acquired with the gradient echo echoplanar imaging and sPRESTO sequences, respectively ( $P>0.05$  for all). Table 3 shows differences in whole-tumor median parameters between children who received a pre-bolus and those who did not.

We found a significant difference between tumor volumes in the low- and high-grade tumor groups (mean±SD = 22.1±23.7 cm<sup>3</sup> and 33.5±28.1 cm<sup>3</sup>;  $P=0.047$ ). Median rCBV<sub>uncorr</sub> was significantly higher in the high-grade tumor group compared to the low-grade tumor group (mean±SD =

**Table 2** Demographics for the 85 children scanned

Diagnosis	n	Gender M/F	Age, yrs. (mean±SD)	Grade(s)	Classification	Center				Mean±SD		Corrected median rCBV	Median $K_2$
						1	2	3	4	Uncorrected median rCBV	Median $K_2$		
Pilocytic astrocytoma	27	13/14	8.3±4.9	1	Low-grade	2	4	8	13	0.13±2.23	1.53±1.24	0.018±0.034	
Medulloblastoma	23	13/10	8.6±4.2	4	High-grade	4	4	5	10	1.80±1.53	2.28±1.17	0.004±0.016	
Anaplastic astrocytoma	3	3/0	10.8±1.7	3	High-grade	-	2	-	1	1.15±0.38	1.26±0.48	0.002±0.004	
Ependymoma <sup>a</sup>	9	3/6	4.8±4.4	2 and 3	High-grade	1	1	1	6	2.60±4.36	2.89±2.75	0.003±0.021	
Central nervous system primitive neuroectodermal tumor	3	3/0	6.1±1.6	4	High-grade	-	-	3	-	4.09±1.63	3.49±1.67	-0.009±0.007	
Oligodendroglioma	3	2/1	11.6±4.8	2	Low-grade	-	-	3	-	3.04±1.66	2.54±1.51	-0.022±0.041	
Other high-grade tumors	7	4/3	7.7±6.3	3 and 4	High-grade	2	-	-	5	3.72±3.08	3.08±1.20	0.001±0.020	
Other low-grade tumors	10	7/3	7.9±6.2	1 and 2	Low-grade	2	1	6	1	-1.81±10.58	1.81±1.64	0.026±0.077	
Total	85	48/37	8.0±4.8			11	12	26	36	1.19±4.41	2.13±1.56	0.009±0.036	

For analysis, the tumors listed here were further divided into five groups of the three most common types included in the study, with all remaining tumors grouped as “other low-grade tumors” and “other high-grade tumors.” Here, the “other high-grade tumor group” includes atypical teratoid rhabdoid tumor ( $n=1$ ), glioblastoma ( $n=2$ ), pineoblastoma ( $n=2$ ) and choroid plexus carcinoma ( $n=2$ ); the “other low-grade tumor group” includes dysembryoplastic neuroepithelial tumor ( $n=2$ ), diffuse astrocytoma ( $n=2$ ), choroid plexus papilloma ( $n=1$ ), atypical choroid plexus papilloma ( $n=1$ ), fibrillary astrocytoma ( $n=1$ ), chordoma ( $n=1$ ), pleomorphic xanthoastrocytoma ( $n=1$ ) and craniopharyngioma ( $n=1$ )

F female,  $K_2$  leakage parameter, M male, rCBV relative cerebral blood volume, SD standard deviation, yrs years

<sup>a</sup>Grade II ependymomas were classified as high-grade tumors because clinically they are treated as malignant tumors [23]

**Table 3** Results of Kruskal-Wallis tests comparing dynamic susceptibility-contrast MRI parameters between children who received any type of contrast agent pre-bolus versus those who did not receive a contrast agent pre-bolus

Pre-bolus contrast agent	Mean±SD		Median $K_2$
	Uncorrected median rCBV	Corrected median rCBV	
Y	1.49±5.48	2.20±1.78	0.016±0.033
N	0.49±2.50	2.04±1.21	0.005±0.039
<i>P</i> -value <sup>a</sup>	<b>0.015</b>	0.978	<b>0.013</b>

$K_2$  leakage parameter, *N* no, *rCBV* relative cerebral blood volume, *SD* standard deviation, *Y* yes

*n*=76 because injection protocol information was not available for 9 children

<sup>a</sup>*P* value <0.05 is significant (bold)

2.37±2.61 vs. -0.14±5.55; *P*=0.008). Median  $rCBV_{\text{corr}}$  was higher in high-grade versus low-grade tumors (mean±SD = 2.54±1.63 vs. 1.68±1.36; *P*=0.01).

Ten of 40 low-grade tumors had negative uncorrected rCBV, a consequence of low rCBV with high contrast agent leakage as seen on post-contrast T1-weighted MR images (Fig. 2). After leakage correction, rCBV increased in 32 of 40 low-grade tumors, including the 10 tumors where rCBV had been negative. Forty-one of 45 high-grade tumors had positive rCBV prior to leakage correction. In 19 high-grade tumors, rCBV decreased indicative of T2\* effects (Fig. 3). Figure 4 shows example uncorrected and corrected signal–time curves for a low- and a high-grade tumor case, respectively. In the low-grade tumor group, a Wilcoxon signed-rank test showed that median whole-tumor rCBV

increased significantly from a mean±SD of -0.14±5.55 to 1.68±1.36 following leakage correction (*P*<0.001); in the high-grade tumor group, median rCBV did not change significantly (mean±SD = 2.37±2.61 vs. 2.54±1.63; *P*=0.307; Fig. 5). Increases in median rCBV averaged across the low- and high-grade groups were 1.81 and 0.17, respectively (*P*=0.060).  $K_2$  was positive in 30 of 40 low-grade tumors, indicating that T1 effects dominated in this group; there was a roughly equal split between positive and negative  $K_2$  in the high-grade tumor group. There was a significant positive correlation between median  $K_2$  and change in rCBV following leakage correction (*r*=0.931, *P*<0.001). Low-grade tumors had significantly higher median  $K_2$  than high-grade tumors (mean±SD = 0.017±0.049 vs. 0.002±0.017; *P*=0.014, Fig. 5).

A Kruskal-Wallis test comparing median dynamic susceptibility-contrast MRI parameters across our five tumor type groupings found that median  $rCBV_{\text{uncorr}}$  was significantly different among tumor types (*P*=0.013; Fig. 6). Post hoc testing showed that this was driven by significant differences between  $rCBV_{\text{uncorr}}$  in pilocytic astrocytomas and medulloblastomas (*P*=0.012) and between pilocytics and other horizontal gene transfer tumors (*P*<0.001). High-grade tumors, including ependymomas and glioblastomas, had the highest values. Pilocytic astrocytomas and other low-grade tumors had the lowest mean values. This significance was lost when leakage correction was applied (*P*=0.124), although  $rCBV_{\text{corr}}$  was statistically significantly different between pilocytic astrocytomas and the “other high-grade tumors” group (*P*=0.026). Median  $K_2$  differed significantly among tumor types (*P*=0.035).  $K_2$  values were highest in pilocytic astrocytomas and again were significantly

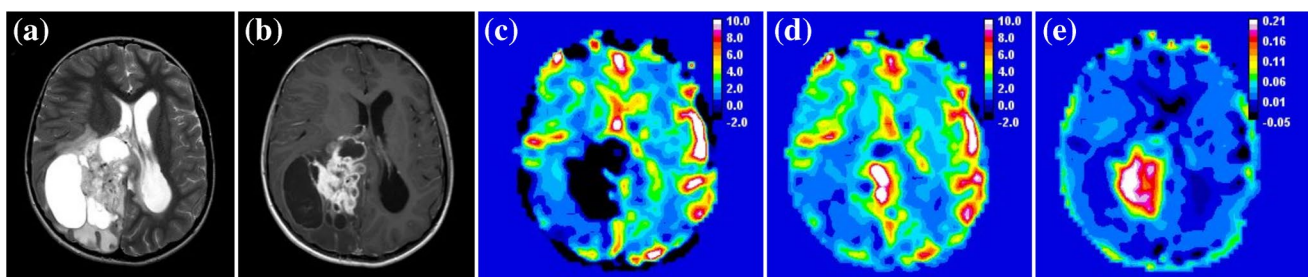


**Fig. 2** Image and maps from a low-grade tumor in an 11-year-5-month-old girl with a pilocytic astrocytoma (classified as grade I) scanned at center 4 on a 1.5-T Achieva (Philips, Best, the Netherlands). **a** Pre-contrast axial T2-weighted MR image (turbo spin-echo sequence, repetition time/echo time [TR/TE] = 6,070/100 ms, number of signals averaged [NSA] = 3, acquired with 4-mm slice thickness and 10% slice gap, reformatted to the dynamic susceptibility-contrast acquisition of 3.5-mm slice thickness, no gap and 3.4×3.4-mm in-plane resolution) on which the tumor region of interest is defined. **b** Post-contrast axial T1-weighted MR image (spin-echo sequence, TR/TE=676/12 ms, NSA=2, acquired with 4-mm slice thickness, 10% gap, reformatted as in (a) shows high signal in

the tumor. **c–e** Uncorrected (**c**) and leakage-corrected (**d**) relative cerebral blood volume (rCBV) maps and  $K_2$  map (**e**) acquired in axial plane. Dynamic susceptibility-contrast data were acquired with an sPRESTO sequence (TR/TE=17/25 ms, flip angle 7°, with 30 slices at 3.4×3.4×3.5-mm resolution). The uncorrected rCBV map shows a black hole indicating negative values in the tumor. After correction, rCBV is shown to increase. The  $K_2$  map shows very high values within the tumor compared to surrounding normal tissue. Uncorrected median rCBV was negative prior to leakage correction (-9.83 vs. 2.97),  $K_2$  was 0.168. sPRESTO sensitivity-encoded Philips principles of echo-shifting with a train of observations

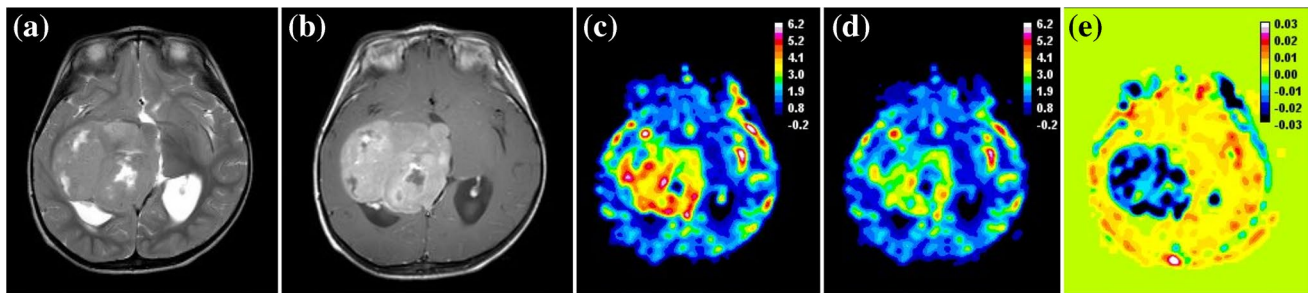


**Fig. 3** Images and maps from a high-grade tumor in a 2-year-old boy with a glioblastoma (classified as grade IV) scanned at center 4 on a 3-T Achieva (Philips, Best, the Netherlands). **a** Pre-contrast axial T2-weighted MR image (turbo spin-echo sequence, repetition time/echo time [TR/TE] = 6,272/85 ms, number of signals averaged [NSA] = 1, acquired with 4-mm slice thickness and 10% gap, reformatted to the dynamic susceptibility-contrast acquisition of 3.5-mm slice thickness, no gap and 1.8×1.8-mm in-plane resolution), on which the tumor region of interest was defined. **b** Post-contrast axial T1-weighted MR image (spin-echo sequence, TR/TE=1,179/14 ms, NSA=1, acquired with 4-mm slice thickness, 10% gap, reformatted as in **(a)**) shows high signal in the tumor. **c–e** Uncorrected **(c)** and leak-

age-corrected **(d)** relative cerebral volume (rCBV) maps and  $K_2$  map **(e)** acquired in the axial plane. Dynamic susceptibility-contrast data were acquired with an sPRESTO sequence (TR/TE=15.9/23.9 ms, flip angle 7°, with 30 slices at 1.8×1.8×3.5-mm resolution). The uncorrected rCBV map shows high values within the tumor. After correction, rCBV is shown to decrease. The  $K_2$  map shows negative values within the tumor compared to surrounding normal tissue. Normalized uncorrected rCBV was high both before and after leakage correction (3.66 vs. 2.68) and  $K_2$  was  $-0.013$ . sPRESTO sensitivity-encoded Philips principles of echo-shifting with a train of observations

different from those in the “other high-grade tumors” group ( $P=0.021$ ), which had the lowest mean value.

Average histograms show whole-tumor uncorrected and corrected rCBV for the three most common tumor types in the study, as well as across the low- and high-grade tumor groups, respectively (Fig. 7). Table 4 shows descriptive parameters, including skew, kurtosis and key percentile values for uncorrected and corrected rCBV along with the significance of differences between the low- and high-grade tumor groups. Pineoblastomas and glioblastomas demonstrated high rCBV (corrected and uncorrected). The lowest rCBV<sub>uncorr</sub> values were found in pilocytic astrocytomas, which also demonstrated the largest increase following leakage correction (from a mean of  $0.13 \pm 2.23$  to  $1.53 \pm 1.24$ ). Sensitivity, specificity, negative and positive predictive values of uncorrected and corrected rCBV and  $K_2$  are summarized in Table 5 for median cut-off values. Receiver operating characteristic curves for rCBV<sub>uncorr</sub> and rCBV<sub>corr</sub> and for  $K_2$  are shown in Fig. 8. Area under the receiver operating characteristic curve values were 0.719, 0.707 and 0.656, respectively. An rCBV<sub>corr</sub> of less than 0.785 had 100% sensitivity for identifying low-grade tumors. In addition, two of the low-grade tumors with the highest rCBV<sub>corr</sub> (4.09 and 2.46) were oligodendrogliomas (grade II). At the time of analysis, the child with the higher rCBV<sub>corr</sub> had died while the other was still alive.

No significant differences were seen between median rCBV<sub>uncorr</sub>, rCBV<sub>corr</sub> and  $K_2$  values measured in children scanned at different centers ( $P>0.05$  in all cases). At center 2, where no pre-bolus was given, rCBV<sub>uncorr</sub> and  $K_2$  were significantly different between the low- and high-grade tumor groups, with no overlap of values ( $P<0.005$  for both

rCBV<sub>uncorr</sub> and  $K_2$ ; Fig. 9). At this center,  $K_2$  was always greater than 0.005 in the low-grade group, with high-grade tumors consistently having values below this. Corrected relative cerebral blood volume was not found to be significantly different between the groups. Using a cut-off value of 0.70, the sensitivity and specificity of rCBV<sub>uncorr</sub> in children scanned at center 2 were both 100%; for rCBV<sub>corr</sub>, they fell to 71% and 80%, respectively, with a cut-off of 1.15; for  $K_2$ , 100% sensitivity and specificity were achieved using a cut-off of 0.005.

## Discussion

We found significant differences in uncorrected and leakage-corrected rCBV when comparing low- and high-grade pediatric brain tumors scanned prior to treatment at multiple centers. This finding is despite large differences in the dynamic susceptibility-contrast MRI protocols employed across centers. While other single-center pediatric studies have shown that rCBV can discriminate between high- and low-grade brain tumors [1, 2, 15, 24, 25], this has not been established in a large multi-center study, and while leakage correction was often used, the results were generally not presented. By analyzing data acquired at multiple centers, we included many children with a variety of tumor types. In particular, pilocytic astrocytomas tended to have low perfusion despite being contrast-enhancing, and an important message of this study is that leakage correction in this tumor group is particularly important if an erroneous rCBV is to be avoided. Overall, these results suggest that, despite differences in dynamic susceptibility-contrast MRI protocols,

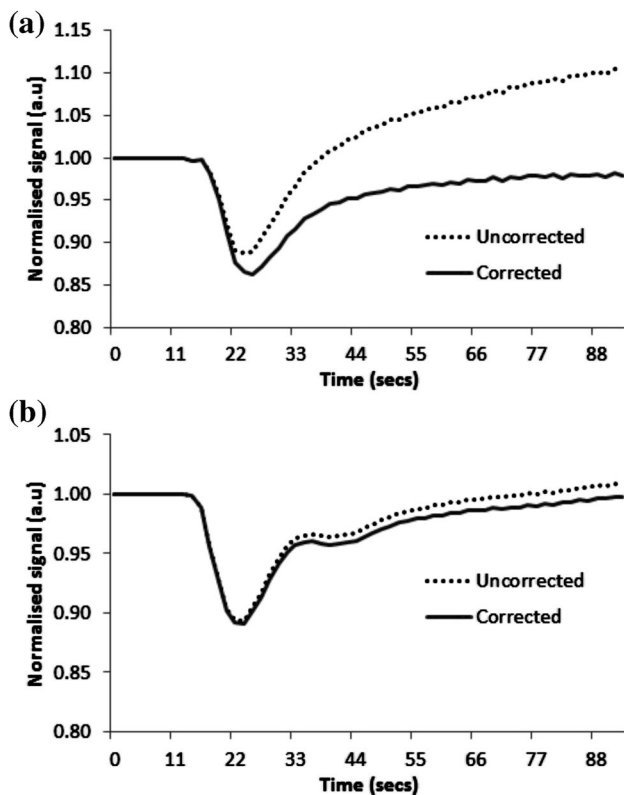


**Fig. 4** Example of signal–time curves from a low-grade tumor and a high-grade tumor, both scanned at center 2 with the same dynamic susceptibility-contrast MRI protocol. No pre-bolus contrast agent was given in either case. The uncorrected and leakage-corrected signal–time curves are shown for both tumors. **a** The low-grade tumor is a grade I pilocytic astrocytoma in a 2-year-10-month-old boy. Uncorrected and corrected median relative cerebral blood volume (rCBV) for the low-grade tumor are  $-0.82$  and  $1.08$ , respectively.  $K_2$  is large and positive at  $0.022$ . **b** The high-grade tumor is a grade IV medulloblastoma in a 5-year-5-month-old boy. Uncorrected and corrected median rCBV for the high-grade tumor are  $1.30$  and  $1.23$ , respectively.  $K_2$  is low at  $0.001$

data can be used to aid clinicians in classifying tumors as low- or high-grade.

Uncorrected rCBV was the most significant parameter for discriminating between high- and low-grade tumors. Low-grade tumors, particularly pilocytic astrocytomas, often had negative rCBV. On applying leakage correction, rCBV became positive, reducing the significance of differences between values in the low- and high-grade tumor groups. Other studies [1, 2] found significantly higher rCBV in high-compared to low-grade tumors. Overlap between values in the two groups in both of those studies as well as ours is extensive, suggesting that dynamic susceptibility-contrast MRI results alone should not be used for tumor grading but should be viewed in conjunction with other MR imaging. Diffusion-weighted imaging in addition to dynamic susceptibility-contrast MRI was found to have high predictive diagnostic accuracy when grading pediatric brain tumors

[15]. In a clinical setting, dynamic susceptibility-contrast MRI should be part of a diagnostic pathway that is refined in a stepwise manner as more information becomes available, starting with clinical history and examination findings, being refined by conventional imaging and then advanced MRI. In this way, perfusion might provide reassurance in the putative diagnosis, or challenge it. In general, the greater the perfusion, the greater the suspicion would be that the tumor is of a high grade.

In Ho et al. [2], pilocytic astrocytomas had the lowest maximum rCBV. High-grade atypical teratoid rhabdoid tumors, medulloblastomas and ependymomas had the highest maximum rCBV. We found that only glioblastomas and pineoblastomas had higher rCBV than ependymomas, with medulloblastomas having the next highest rCBV. A previous study showed that of all gliomas included, glioblastomas had the highest maximum white-matter-normalized rCBV,  $7.32$  [26]. Some tumor groups in our study were limited in number and so results should be treated with caution. Medulloblastomas had a large range of rCBV values, possibly because of differences in molecular subgroups [27]. Ho et al. [2] also presented average histograms of rCBV for different tumor types, showing that pilocytic astrocytomas had a higher proportion of low rCBV values than high-grade tumors including ependymomas and medulloblastomas. Similarly, we found differences between rCBV histogram centiles. As in Ho's study, skew and kurtosis did not differ significantly between the low- and high-grade groups in our study, suggesting that while histograms from different tumor types might differ in shape, when taken over a larger population, these differences are not significant.

Another study [24] did not employ leakage correction but classified dynamic susceptibility-contrast MRI signal–time courses as having no leakage, T1- or T2\*-dominant leakage depending on whether they returned to baseline, continued above baseline or failed to return to baseline, respectively. Sensitivity tests found that a T1-dominant leakage pattern predicted lateral gene transfer in 66% of cases, rising to 91% in pilocytic astrocytomas; a T2\*-dominant or baseline pattern predicted horizontal gene transfer in 100% of cases. We found median  $rCBV_{corr}$  had the highest sensitivity (76%) and specificity (65%) for detecting high-grade tumors using a cut-off of  $1.70$ . A threshold of  $1.60$  for  $rCBV_{uncorr}$  resulted in reduced sensitivity (53%) while specificity was improved (83%). These cut-off values lie above and below the  $1.38$  for maximum rCBV found in Ho et al. [2] and  $1.07$  for rCBV resulting in 100% sensitivity found by Dallery et al. [1], but they are close to the  $1.75$  cut-off presented by Law et al. [28] when grading adult gliomas. The low sensitivity and specificity found in our study again emphasize the importance of not using these as single tests but rather as adding information to other clinical and imaging characteristics to achieve the most likely noninvasive diagnosis, with rCBV values well above

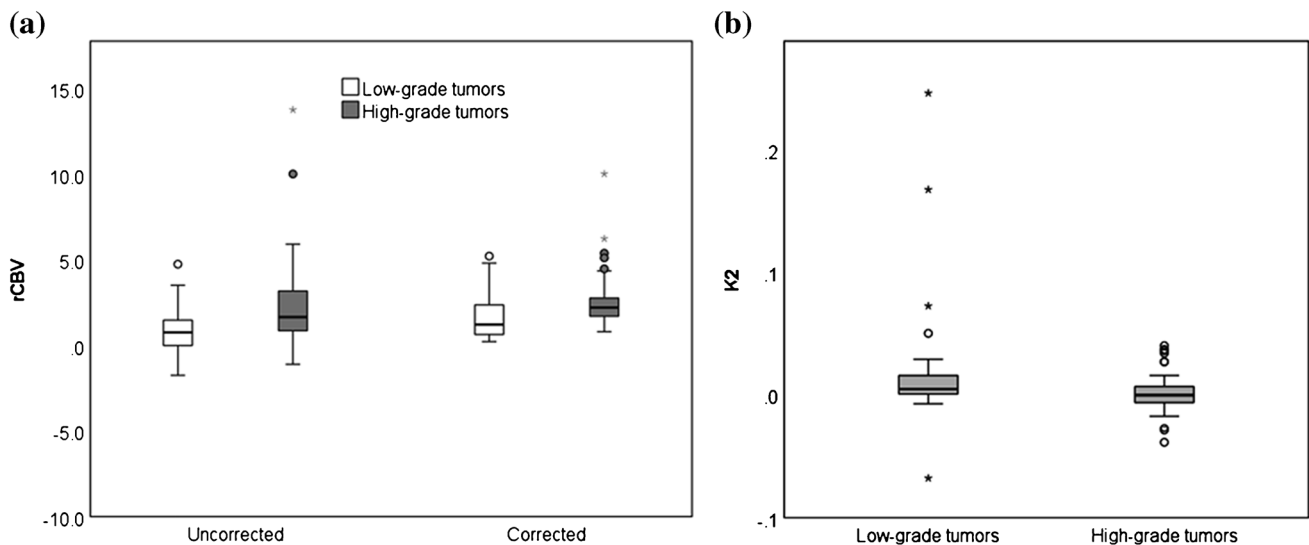


**Fig. 5** Boxplots show parameter distributions across the high-grade and low-grade tumor groups, respectively. **a, b** Median uncorrected relative cerebral blood volume ( $rCBV_{uncorr}$ ) and corrected relative cerebral blood volume ( $rCBV_{corr}$ ) (**a**) and median  $K_2$  (**b**). The bold lines show the mean parameter, whiskers show the interquartile range. The

$P$ -values from the Kruskal-Wallis tests for significant differences in parameters between the high-grade and low-grade tumor groups were significant at 0.008, 0.010 and 0.014 for  $rCBV_{uncorr}$ ,  $rCBV_{corr}$  and  $K_2$ , respectively

or below the cut-off having more influence. While cases that have an  $rCBV_{corr}$  close to the cut-off cannot be confidently assigned as low- or high-grade, those with a value below 0.785 are highly likely to be a low-grade tumor. Similarly, tumors with an  $rCBV_{corr}$  that is much higher than the cut-off might have an aggressive phenotype even if low-grade, as seen in the two oligodendrogliomas, known to be the more aggressive of pediatric low-grade tumors. It could be that dynamic susceptibility-contrast MRI parameters give prognostic information, as has been shown in other pediatric studies [4].

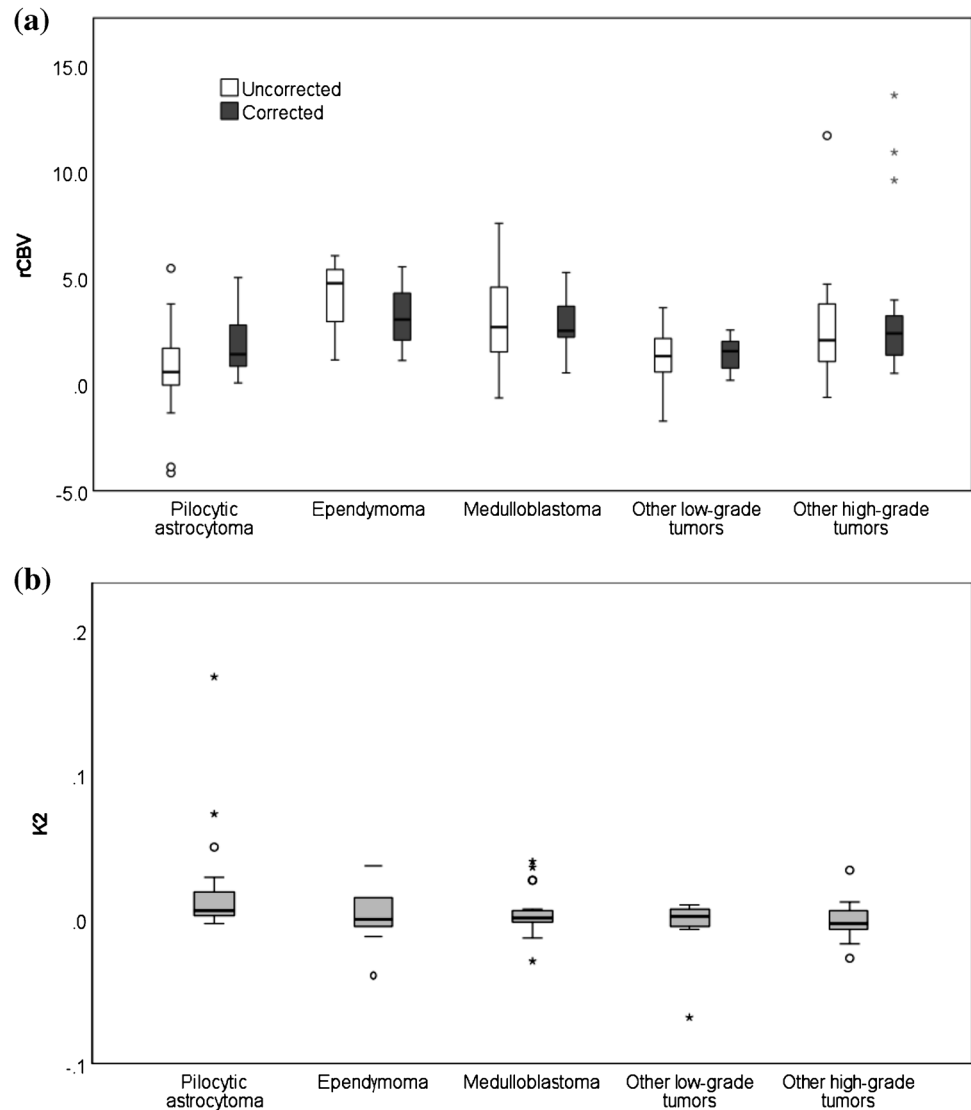
Only one pediatric study has presented  $K_2$  results. Provenzale et al. [25] found that  $K_2$  was significantly higher in high-grade than in low-grade tumors. This contradicts our results, although the leakage-correction model used [10] differs from ours [9] in not including correction for T2\*-dominant effects. In Liu et al. [9], T1-dominant tumors had higher, positive  $K_2$  values whereas T2\*-dominant tumors had lower, often negative,  $K_2$  values. In agreement with Dallery et al. [1], pilocytic astrocytomas demonstrated significant T1 effects, suggesting that  $K_2$  should be raised in these tumors.  $K_2$  provides a measure of the amount of leakage correction that has been applied and so will be reduced by the administration of a pre-bolus of contrast agent. It is known to depend on sequence parameters (TR, TE), pre-contrast T1 value, blood volume and permeability–surface area product. Studies have shown that  $K_2$  correlates well with  $K_{trans}$  obtained from dynamic contrast-enhanced MRI [29], which represents a combination of permeability–surface area product and blood flow [30].

$K_2$  and  $rCBV_{uncorr}$  had lower sensitivity and specificity than  $rCBV_{corr}$ , likely caused by differences in injection protocols

and the need to correct for negative  $rCBV_{uncorr}$  values. Leakage correction is therefore essential to improve the accuracy of  $rCBV$  values and to account for differences in injection protocols across a pooled dataset such as this, improving the differentiation of the low- and high-grade groups. Uncorrected relative cerebral blood volume and  $K_2$  should be treated with caution unless injection protocols are consistent across the patient population. While we have presented thresholds that maximize the sensitivity and specificity at identifying high-grade tumors across this whole dataset, thresholds vary with the protocol used and so the optimal threshold should be established on a site-by-site basis.

Previous studies recommended administering a pre-bolus of contrast agent to minimize T1 effects in enhancing brain tumors that result in underestimation of uncorrected  $rCBV$  [6, 7]. While a pre-load of contrast agent reduces the effects of leakage, it does not eliminate them. This is particularly the case in the pediatric population, where administration of a single dose of gadolinium is recommended, being split between the pre-bolus and the main bolus. Consequently, if the size of the pre-bolus is increased, then leakage effects are more successfully suppressed but the size of the main bolus is reduced, leading to a reduced signal drop to noise ratio of the time-course. Use of leakage correction reduces the variability that results from the use of different pre-bolus volumes and is particularly useful if  $rCBV$  is to be compared across multiple protocols employing different extents of leakage suppression by use of a pre-bolus, as in our study.  $K_2$  and  $rCBV_{uncorr}$  depend on the size of pre-bolus given, whereas a leakage-corrected  $rCBV$  should be more robust,

**Fig. 6** Boxplots show distribution of (a) median uncorrected relative cerebral blood volume ( $rCBV_{uncorr}$ ) and corrected relative cerebral blood volume ( $rCBV_{corr}$ ) and (b) median  $K_2$  across three common tumor types, with other tumors grouped as “other high-grade tumors” or “other low-grade tumors.” The  $P$ -values from Kruskal-Wallis tests were significant at 0.001, 0.006 and 0.035, respectively



and in pooled data with multiple injection protocols, leakage correction is essential to provide comparable data.

One center in our study consistently did not employ a pre-bolus of contrast agent. Leakage-uncorrected  $rCBV$  in the high- and low-grade tumor groups from this center had the best separation and highest significance using a cut-off of 0.70.  $K_2$  was always greater than 0.005 in low-grade tumors, with high-grade tumors consistently having values below this, suggesting that  $K_2$  can differentiate between low- and high-grade tumors and might hold valuable information if comparing across a dataset with consistent injection protocols. These results, while interesting, should be viewed with caution — only 12 children were scanned at this center, although there was a good split between low-grade ( $n=5$ ) and high-grade ( $n=7$ ) tumors. We also suggest that a pre-bolus of contrast agent is not necessary if leakage correction is applied and that administering a pre-bolus affects  $K_2$  values by compensating for leakage correction. It was recently reported [31]

that a pre-bolus might not be necessary in adult brain tumors and that a low-flip-angle protocol with leakage correction might be preferable [32]. In our study, children who received a pre-bolus of contrast agent had increased uncorrected  $rCBV$  (suggesting a reduction in T1 leakage effects) and reduced  $K_2$  (indicating reduced need for leakage correction). Leakage correction reduced differences in  $rCBV$  from injection protocol. It should be noted that we did not test for all differences in injection protocols, comparing only between those who received a pre-bolus and those who did not.

While too many differences exist between the dynamic susceptibility-contrast MRI protocols in this study to draw any conclusions regarding protocol optimization, certain factors (field strength and pulse sequence) did not result in significant differences between parameters obtained across the dataset. This suggests that differences in median parameters between high and low tumor grading are greater than those introduced by the variation in scan protocols.

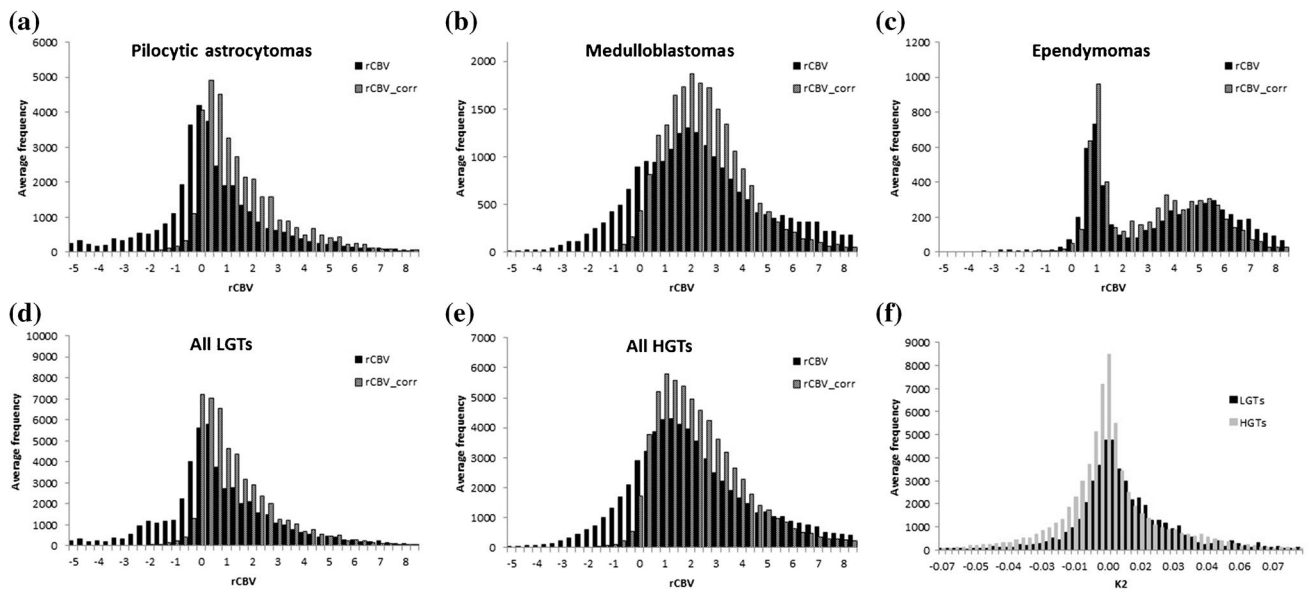


**Fig. 7** Mean histograms show the distribution of uncorrected and corrected relative cerebral blood volume (rCBV) averaged over (a) all pilocytic astrocytomas ( $n=27$ ), (b) all medulloblastomas ( $n=23$ ), (c) all ependymomas ( $n=9$ ), (d) all other low-grade tumors (LGTs)

( $n=10$ ), (e) all other high-grade tumors (HGTs) ( $n=7$ ) and (f) the distribution of the leakage parameter ( $K_2$ ) averaged over the low- and high-grade tumor groups, respectively

Data in this study were acquired at multiple centers with variable protocols, creating challenges for data analysis. Thirty-two datasets were excluded because of technical issues — data corruption, incomplete data and poor quality. While the sPRESTO and gradient echo echoplanar imaging sequences produced comparable cerebral blood volumes in simulations and animal studies [18], poor temporal stability has been observed with the sPRESTO sequence [33]. Signal-to-noise ratio was variable between protocols, reduced by use of a pre-bolus and low flip angle, while the use of 3 T and no pre-bolus boosted signal-to-noise ratio. Trade-offs were made between spatial resolution and whole-head coverage versus temporal resolution and signal-to-noise ratio. All centers administered a standard single dose of contrast agent in line with current recommendations [17]. Reproducibility of parameters from regions of interest defined by two users suggests that region definition can be undertaken by multiple users across centers. We defined regions of interest encompassing the whole tumor to investigate differences in whole-tumor median parameters as well as the distributions of parameters across the tumor. Other studies have measured rCBV in hot spots, showing significant differences in maximal perfusion in the tumor. Choosing a hot spot is subject to location, being affected by both protocol and analysis method, and has a risk of being unduly affected by artifacts [5]; therefore, we expect a whole-tumor method to be more robust in a multicenter study. Finally, there were three versions of the World Health Organization guidance on classifying central nervous system tumors over the long accrual period in this study [19–21]. Tumors were classified according to the guidance available at the time. Tumor gradings were not affected by any changes.

In recent years, there have been concerns about the use of gadolinium contrast agents. People with poor renal function have been shown to be at risk of developing nephrogenic systemic fibrosis following gadolinium exposure [34], while recent studies have shown increased signal caused by T1 shortening on MRI scans from contrast agent deposition in areas of the brain including the dentate nucleus and globus pallidus [35] following earlier exposure to gadolinium. Children are at low risk of nephrogenic systemic fibrosis [36]; however, there are concerns about the long-term effects of gadolinium deposition in children's brains, particularly in those undergoing repeated MR examinations with contrast agents [37]. Guidance mandates use of macrocyclic rather than linear agents to minimize risks, the use of single dose titrated by weight, and risk-versus-benefit analysis before prescribing contrast agent, with consideration given to non-contrast methods [38]. In patient groups such as children with brain tumors, it is still recommended that a single-dose contrast agent be administered during MRI scans at diagnosis and follow-up for acquisition of post-contrast conventional MRI [17] and, while this remains the case, acquiring dynamic susceptibility-contrast MRI after the contrast injection has no added risks compared to the routine imaging. Indeed, it provides an efficient use of resources. A power injector is recommended for reproducible administration of contrast agent during dynamic susceptibility-contrast MRI [17, 32]. This requires venous access via a cannula, which is invasive and can be tricky, particularly in children [39]. The majority of our pediatric brain tumor patients have a cannula in situ at the time of their staging scan or because they are undergoing an MRI under general anesthetic.

**Table 4** Results of the Kruskal-Wallis test comparing parameters describing the distribution of uncorrected and corrected relative cerebral blood volume (rCBV) obtained from whole-tumor regions of interest between the low- and high-grade tumor groups

Parameters <sup>a</sup>	Tests between low- and high-grade tumor groups					
	Uncorrected rCBV			Corrected rCBV		
	Low-grade (mean±SD)	High-grade (mean±SD)	<i>P</i> -value <sup>b</sup>	Low-grade (mean±SD)	High-grade (mean±SD)	<i>P</i> -value <sup>b</sup>
Skew	0.94±1.05	0.89±0.72	0.725	1.25±1.11	1.01±0.80	0.573
Kurtosis	3.34±3.80	3.04±2.99	0.809	4.42±6.11	2.98±2.99	0.403
10th percentile	-2.08±6.82	0.36±2.05	<b>0.000</b>	-0.20±2.34	-0.86±1.09	0.154
25th percentile	-1.19±6.21	1.33±2.22	<b>0.000</b>	0.43±2.61	-0.37±0.98	0.108
75th percentile	1.18±4.76	3.51±3.23	<b>0.002</b>	1.60±3.19	0.66±1.18	<b>0.011</b>
90th percentile	2.53±4.19	4.75±3.99	<b>0.008</b>	2.13±3.39	1.11±1.40	<b>0.012</b>
Minimum	-5.19±9.67	-3.00±3.74	0.117	-0.84±2.09	-0.82±2.41	0.285
Maximum	8.43±6.19	12.00±9.02	<b>0.035</b>	8.18±6.61	9.86±8.51	0.150

rCBV relative cerebral blood volume, SD standard deviation

<sup>a</sup>Parameters include the skew and kurtosis in rCBV across the whole tumor, along with the values of percentiles obtained, for example, the 10th percentile value is the value below which 10% of all values in the whole-tumor region of interest lie

<sup>b</sup>*P*-value <0.05 is significant (bold)

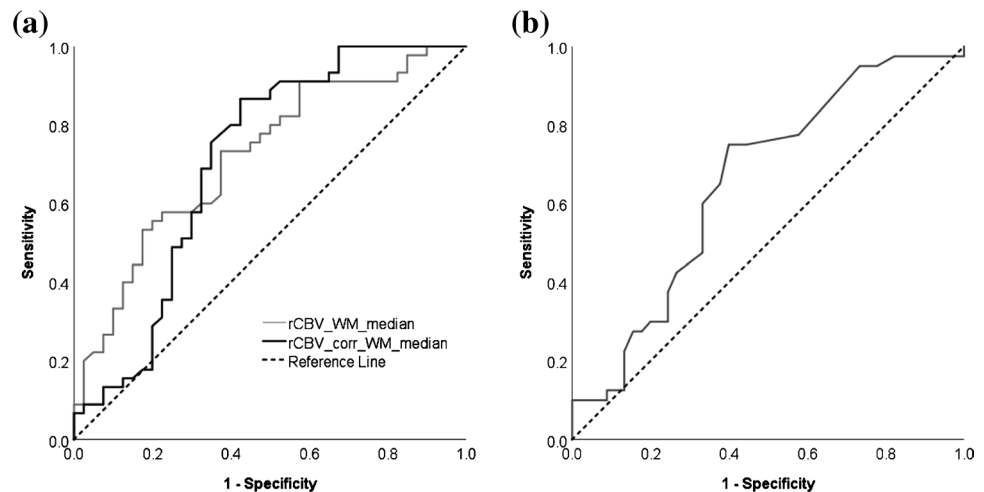
**Table 5** Mean parameters for the low- and high-grade tumor groups, respectively, along with 95% confidence intervals; cut-off values for differentiating between low- and high-grade tumors are shown along-

side the specificity, sensitivity, positive and negative predictive values of each parameter when this cut-off is employed

Whole-tumor median of parameter	Grade	Mean	95% confidence interval for mean	Cut-off value	Sensitivity (%)	Specificity (%)	Positive predictive value (%)	Negative predictive value (%)
Uncorrected rCBV	Low-grade	-0.14	-1.91–1.64	1.60	53.3	82.5	77.4	61.1
	High-grade	2.37	1.58–3.15					
Corrected rCBV	Low-grade	1.68	1.24–2.11	1.70	75.6	65.0	70.8	70.3
	High-grade	2.54	2.05–3.03					
K <sub>2</sub>	Low-grade	0.017	0.002–0.033	0.001	60.0	75.0	73.0	62.5
	High-grade	0.002	-0.003–0.007					

K<sub>2</sub> leakage parameter, rCBV relative cerebral blood volume

**Fig. 8** Receiver operating characteristic curves for dynamic susceptibility-contrast MRI parameters to compare performance in discriminating between high- and low-grade tumors. **a, b** Receiver operating characteristic curves for median uncorrected relative cerebral blood volume (rCBV<sub>uncorr</sub>) and corrected relative cerebral blood volume (rCBV<sub>corr</sub>) (**a**) and median K<sub>2</sub> (**b**). The area under the receiver operating characteristic curve values for the parameters were 0.719, 0.707 and 0.656, respectively. WM white matter



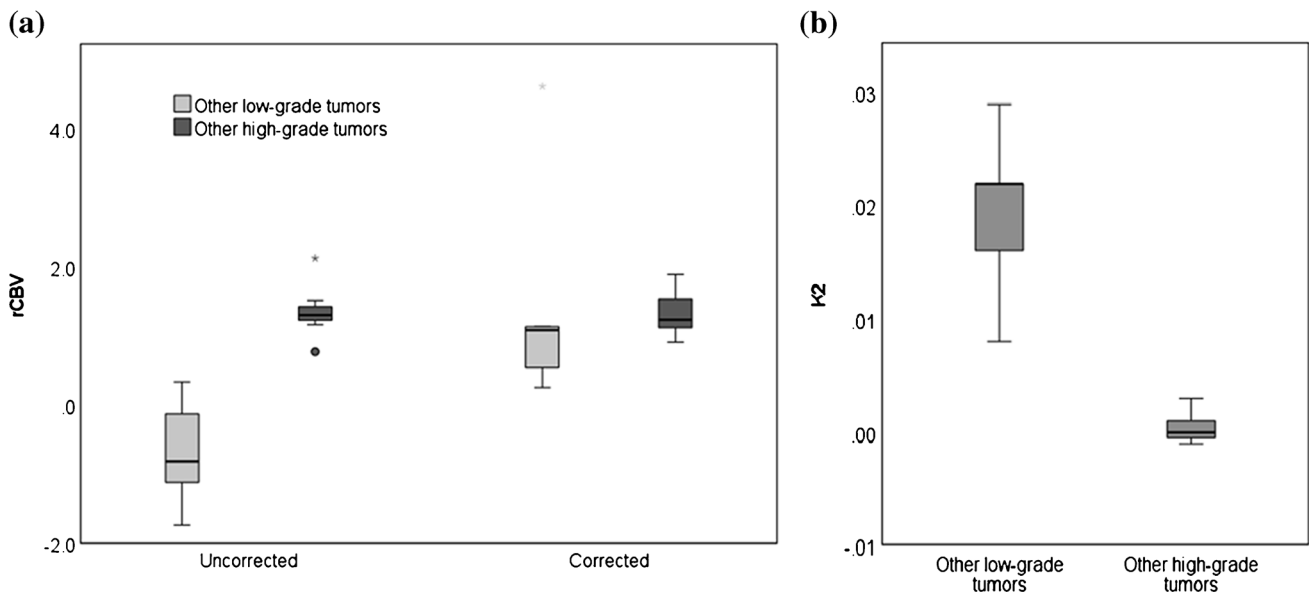


**Fig. 9** Boxplots show parameter distributions across the high-grade and low-grade tumor groups, respectively, for center 2. At center 2, children routinely did not receive a pre-bolus of contrast agent. **a** Median uncorrected relative cerebral blood volume ( $rCBV_{uncorr}$ ) and corrected relative cerebral blood volume ( $rCBV_{corr}$ ). **b** Median  $K_2$ .

Arterial spin-labeling measures perfusion without the need for a contrast agent. It has been shown to agree with dynamic susceptibility-contrast MRI measures of perfusion in children [40], with increased perfusion observed in high-grade pediatric brain tumors compared to low-grade tumors [14]. It is gaining popularity as a method, particularly in populations at risk of nephrogenic systemic fibrosis or in those undergoing repeat MRIs. However, in comparison to dynamic susceptibility-contrast MRI, it suffers from long scan times, low signal-to-noise ratio and poor spatial resolution, and leakage information, shown to be of use in this study, is not available. Arterial spin labeling is difficult in children because of age-related variations in blood flow. While there is a recommended protocol for clinical applications in adults [41], this method is difficult in children, where the optimal post-labeling delay required has been shown to vary with age [42]. Other advanced MRI methods, including MR spectroscopy and diffusion-weighted MRI, have also been shown to provide information on tumor grading in pediatric brain tumors [43].

## Conclusion

Despite difficulties in dealing with multicenter data, we have shown that rCBV values derived from dynamic susceptibility-contrast MRI data acquired at multiple centers can be used to help discriminate between high- and low-grade pediatric brain tumors. Perfusion parameters varied with tumor

type but not with center. Low-grade tumors had significantly lower rCBV than high-grade tumors, requiring leakage correction to counteract T1-dominant effects. Thresholds using the median parameter of 1.60 and 1.70 for uncorrected and corrected rCBV, respectively, gave moderate sensitivity and specificity for identifying high-grade tumors. Dynamic susceptibility-contrast MRI without a pre-bolus of contrast agent gave improved sensitivity and specificity for  $rCBV_{uncorr}$  and  $K_2$  in a small subset of children, suggesting that a pre-bolus could be omitted in this population. Leakage-corrected dynamic susceptibility-contrast MRI in conjunction with conventional MRI and other advanced MR techniques, such as diffusion-weighted imaging and spectroscopy, might aid in early grading of pediatric brain tumors.

**Acknowledgments** We would like to acknowledge funding from the Cancer Research UK and EPSRC Cancer Imaging Programme at the Children’s Cancer and Leukaemia Group (CCLG) in association with the MRC and Department of Health (England) (C7809/A10342), the Cancer Research UK and NIHR Experimental Cancer Medicine Centre Paediatric Network (C8232/A25261), Health Data Research UK (HDR UK) and Help Harry Help Others charity. Prof. Peet is funded through an NIHR Research Professorship, NIHR-RP-R2-12-019. Stephen Powell gratefully acknowledges financial support from EPSRC through a studentship from the Physical Sciences for Health Centre for Doctoral Training (EP/L016346/1). Prof. Theodoros N. Arvanitis is partially funded by HDR UK. HDR UK is funded by the UK Medical Research Council, Engineering and Physical Sciences Research Council, Economic and Social Research Council, Department of Health and Social Care (England), Chief Scientist Office of the Scottish Government Health and Social Care Directorates, Health and Social Care Research and Development Division (Welsh Government), Public Health Agency

(Northern Ireland), British Heart Foundation and Wellcome Trust. We would also like to thank the MR radiographers at Birmingham Children's Hospital, Alder Hey Children's Hospital, the Royal Victoria Infirmary in Newcastle and Nottingham Children's Hospital for scanning the patients in this study; Selene Rowe at Nottingham University Hospitals NHS Trust for help with gaining MRI protocol information and Jane Crouch at Birmingham Children's Hospital for help with getting tumor diagnoses and patient information.

## Declarations

**Conflicts of interest** None

**Open Access** This article is licensed under a Creative Commons Attribution 4.0 International License, which permits use, sharing, adaptation, distribution and reproduction in any medium or format, as long as you give appropriate credit to the original author(s) and the source, provide a link to the Creative Commons license, and indicate if changes were made. The images or other third party material in this article are included in the article's Creative Commons license, unless indicated otherwise in a credit line to the material. If material is not included in the article's Creative Commons license and your intended use is not permitted by statutory regulation or exceeds the permitted use, you will need to obtain permission directly from the copyright holder. To view a copy of this license, visit <http://creativecommons.org/licenses/by/4.0/>.

## References

- Dallery F, Bouzerar R, Michel D et al (2017) Perfusion magnetic resonance imaging in pediatric brain tumors. *Neuroradiology* 59:1143–1153
- Ho CY, Cardinal JS, Kamer AP, Kralik SF (2015) Relative cerebral blood volume from dynamic susceptibility contrast perfusion in the grading of pediatric primary brain tumors. *Neuroradiology* 57:299–306
- Schmainda KM, Prah M, Connelly J et al (2014) Dynamic-susceptibility contrast agent MRI measures of relative cerebral blood volume predict response to bevacizumab in recurrent high-grade glioma. *Neuro Oncol* 16:880–888
- Hipp SJ, Steffen-Smith E, Hammoud D et al (2011) Predicting outcome of children with diffuse intrinsic pontine gliomas using multiparametric imaging. *Neuro Oncol* 13:904–909
- Paulson ES, Schmainda KM (2008) Comparison of dynamic susceptibility-weighted contrast-enhanced MR methods: recommendations for measuring relative cerebral blood volume in brain tumors. *Radiology* 249:601–613
- Leu K, Boxerman JL, Ellingson BM (2017) Effects of MRI protocol parameters, preload injection dose, fractionation strategies, and leakage correction algorithms on the fidelity of dynamic-susceptibility contrast MRI estimates of relative cerebral blood volume in gliomas. *AJNR Am J Neuroradiol* 38:478–484
- Hu LS, Baxter LC, Pinnaduwage DS et al (2010) Optimized preload leakage-correction methods to improve the diagnostic accuracy of dynamic susceptibility-weighted contrast-enhanced perfusion MR imaging in posttreatment gliomas. *AJNR Am J Neuroradiol* 31:40–48
- Boxerman JL, Schmainda KM, Weisskoff RM (2006) Relative cerebral blood volume maps corrected for contrast agent extravasation significantly correlate with glioma tumor grade, whereas uncorrected maps do not. *AJNR Am J Neuroradiol* 27:859–867
- Liu HL, Wu YY, Yang WS et al (2011) Is Weisskoff model valid for the correction of contrast agent extravasation with combined T1 and T2\* effects in dynamic susceptibility contrast MRI? *Med Phys* 38:802–809
- Weisskoff RM (1994) Simultaneous blood volume and permeability mapping using a single Gd-based contrast injection. *International Society for Magnetic Resonance in Medicine, Concord*
- Rashed WM, Maher E, Adel M et al (2019) Pediatric diffuse intrinsic pontine glioma: where do we stand? *Cancer Metastasis Rev* 38:759–770
- Manias K, Gill SK, Zarinabad N et al (2018) Evaluation of the added value of (1)H-magnetic resonance spectroscopy for the diagnosis of pediatric brain lesions in clinical practice. *Neurooncol Pract* 5:18–27
- Novak J, Zarinabad N, Rose H et al (2021) Classification of paediatric brain tumours by diffusion weighted imaging and machine learning. *Sci Rep* 11:2987
- Yeom KW, Mitchell LA, Lober RM et al (2014) Arterial spin-labeled perfusion of pediatric brain tumors. *AJNR Am J Neuroradiol* 35:395–401
- Koob M, Girard N, Ghattas B et al (2016) The diagnostic accuracy of multiparametric MRI to determine pediatric brain tumor grades and types. *J Neurooncol* 127:345–353
- Children's Cancer and Leukaemia Group (CCLG) Functional imaging database (2021) <https://www.cclg.org.uk/>. Accessed 4 Oct 2021
- European Society for Paediatric Oncology (SIOP) (2017) Imaging protocol for patients in European SIOP brain tumour studies. [https://pho.barnlakarforeningen.se/wp-content/uploads/sites/20/2019/05/VCTB\\_radiologi-Imaging-protocol-for-patients-in-European-SIOP-Brain-Tumour-Studies\\_Dec-2017.pdf](https://pho.barnlakarforeningen.se/wp-content/uploads/sites/20/2019/05/VCTB_radiologi-Imaging-protocol-for-patients-in-European-SIOP-Brain-Tumour-Studies_Dec-2017.pdf). Accessed 4 Oct 2021
- Pedersen M, Klarhofer M, Christensen S et al (2004) Quantitative cerebral perfusion using the PRESTO acquisition scheme. *J Magn Reson Imaging* 20:930–940
- Kleihues P, Louis DN, Scheithauer BW et al (2002) The WHO classification of tumors of the nervous system. *J Neuropathol Exp Neurol* 61:215–225
- Louis DN, Ohgaki H, Wiestler OD et al (2007) The 2007 WHO classification of tumours of the central nervous system. *Acta Neuropathol* 114:97–109
- Louis DN, Perry A, Reifenberger G et al (2016) The 2016 World Health Organization classification of tumors of the central nervous system: a summary. *Acta Neuropathol* 131:803–820
- Rorden C, Brett M (2000) Stereotaxic display of brain lesions. *Behav Neurol* 12:191–200
- Leeper H, Felicella MM, Walbert T (2017) Recent advances in the classification and treatment of ependymomas. *Curr Treat Options Oncol* 18:55
- Ho CY, Cardinal JS, Kamer AP et al (2016) Contrast leakage patterns from dynamic susceptibility contrast perfusion MRI in the grading of primary pediatric brain tumors. *AJNR Am J Neuroradiol* 37:544–551
- Provenzale JM, Wang GR, Brenner T et al (2002) Comparison of permeability in high-grade and low-grade brain tumors using dynamic susceptibility contrast MR imaging. *AJR Am J Roentgenol* 178:711–716
- Sugahara T, Korogi Y, Kochi M et al (1998) Correlation of MR imaging-determined cerebral blood volume maps with histologic and angiographic determination of vascularity of gliomas. *AJR Am J Roentgenol* 171:1479–1486
- Schwalbe EC, Lindsey JC, Nakjang S et al (2017) Novel molecular subgroups for clinical classification and outcome prediction in childhood medulloblastoma: a cohort study. *Lancet Oncol* 18:958–971

28. Law M, Yang S, Wang H et al (2003) Glioma grading: sensitivity, specificity, and predictive values of perfusion MR imaging and proton MR spectroscopic imaging compared with conventional MR imaging. *AJNR Am J Neuroradiol* 24:1989–1998
29. Taoka T, Kawai H, Nakane T et al (2016) Application of histogram analysis for the evaluation of vascular permeability in glioma by the K2 parameter obtained with the dynamic susceptibility contrast method: comparisons with Ktrans obtained with the dynamic contrast enhance [sic] method and cerebral blood volume. *Magn Reson Imaging* 34:896–901
30. Donaldson SB, West CM, Davidson SE et al (2010) A comparison of tracer kinetic models for T1-weighted dynamic contrast-enhanced MRI: application in carcinoma of the cervix. *Magn Reson Med* 63:691–700
31. Schmainda KM, Prah MA, Hu LS et al (2019) Moving toward a consensus DSC-MRI protocol: validation of a low-flip angle single-dose option as a reference standard for brain tumors. *AJNR Am J Neuroradiol* 40:626–633
32. Welker K, Boxerman J, Kalnin A et al (2015) ASFNR recommendations for clinical performance of MR dynamic susceptibility contrast perfusion imaging of the brain. *AJNR Am J Neuroradiol* 36:E41–E51
33. van Gelderen P, Duyn JH, Ramsey NF et al (2012) The PRESTO technique for fMRI. *Neuroimage* 62:676–681
34. Grobner T (2006) Gadolinium — a specific trigger for the development of nephrogenic fibrosing dermopathy and nephrogenic systemic fibrosis? *Nephrol Dial Transplant* 21:1104–1108
35. Kanda T, Ishii K, Kawaguchi H et al (2014) High signal intensity in the dentate nucleus and globus pallidus on unenhanced T1-weighted MR images: relationship with increasing cumulative dose of a gadolinium-based contrast material. *Radiol* 270:834–841
36. Nardone B, Saddleton E, Laumann AE et al (2014) Pediatric nephrogenic systemic fibrosis is rarely reported: a RADAR report. *Pediatr Radiol* 44:173–180
37. Rozenfeld MN, Podberesky DJ (2018) Gadolinium-based contrast agents in children. *Pediatr Radiol* 48:1188–1196
38. Royal College of Radiologists (2019) Guidance on gadolinium-based contrast agent administration to adult patients. Royal College of Radiologists, London
39. Gholkar MS (2005) Cannulating children. *Br J Med* 330:s135
40. Novak J, Withey SB, Lateef S et al (2019) A comparison of pseudo-continuous arterial spin labelling and dynamic susceptibility contrast MRI with and without contrast agent leakage correction in paediatric brain tumours. *Br J Radiol* 92:20170872
41. Alsop DC, Detre JA, Golay X et al (2015) Recommended implementation of arterial spin-labeled perfusion MRI for clinical applications: a consensus of the ISMRM perfusion study group and the European consortium for ASL in dementia. *Magn Reson Med* 73:102–116
42. Tang S, Liu X, He L et al (2019) Application of postlabeling delay time in 3-dimensional pseudocontinuous arterial spin-labeled perfusion imaging in normal children. *J Comput Assist Tomogr* 43:697–707
43. Hales PW, d'Arco F, Cooper J et al (2019) Arterial spin labelling and diffusion-weighted imaging in paediatric brain tumours. *Neuroimage Clin* 22:101696

**Publisher's note** Springer Nature remains neutral with regard to jurisdictional claims in published maps and institutional affiliations.

## Authors and Affiliations

Stephanie B. Withey<sup>1,2,3</sup> · Lesley MacPherson<sup>4</sup> · Adam Oates<sup>4</sup> · Stephen Powell<sup>3</sup> · Jan Novak<sup>2,3,5</sup> · Laurence Abernethy<sup>6</sup> · Barry Pizer<sup>7</sup> · Richard Grundy<sup>8</sup> · Paul S. Morgan<sup>8,9,10</sup> · Simon Bailey<sup>11</sup> · Dipayan Mitra<sup>12</sup> · Theodoros N. Arvanitis<sup>2,3,13</sup> · Dorothee P. Auer<sup>10,14,15</sup> · Shivaram Avula<sup>6</sup> · Andrew C. Peet<sup>2,3,16</sup> 

<sup>1</sup> RRPBS, University Hospitals Birmingham NHS Foundation Trust, Birmingham, UK

<sup>2</sup> Oncology, Birmingham Women's and Children's NHS Foundation Trust, Birmingham, UK

<sup>3</sup> Institute of Cancer and Genomic Sciences, University of Birmingham, Birmingham, UK

<sup>4</sup> Radiology, Birmingham Women's and Children's NHS Foundation Trust, Birmingham, UK

<sup>5</sup> Department of Psychology, Aston Brain Centre, School of Life and Health Sciences, Aston University, Birmingham, UK

<sup>6</sup> Radiology, Alder Hey Children's NHS Foundation Trust, Liverpool, UK

<sup>7</sup> Oncology, Alder Hey Children's NHS Foundation Trust, Liverpool, UK

<sup>8</sup> The Children's Brain Tumour Research Centre, University of Nottingham, Nottingham, UK

<sup>9</sup> Medical Physics, Nottingham University Hospitals, Nottingham, UK

<sup>10</sup> Division of Clinical Neuroscience, School of Medicine, University of Nottingham, Nottingham, UK

<sup>11</sup> Sir James Spence Institute of Child Health, Royal Victoria Infirmary, Newcastle upon Tyne, UK

<sup>12</sup> Neuroradiology, Royal Victoria Infirmary, Newcastle upon Tyne, UK

<sup>13</sup> Institute of Digital Healthcare, WMG, University of Warwick, Coventry, UK

<sup>14</sup> Neuroradiology, Nottingham University Hospitals Trust, Nottingham, UK

<sup>15</sup> NIHR Nottingham Biomedical Research Centre, Nottingham, UK

<sup>16</sup> Children's Brain Tumour Research Team, 4th Floor Institute of Child Health, Birmingham Women's and Children's Hospital NHS Foundation Trust, Steelhouse Lane, Birmingham B4 6NH, UK